Effect of Detailed Power System Models in Traditional and Voltage Stability Constrained Optimal Power Flow Problems

William Rosehart, *Member, IEEE*, Claudio A. Cañizares, *Senior Member, IEEE*, and Victor H. Quintana, *Fellow, IEEE*

Abstract— **In this paper, detailed generator, exponential load and Static VAR Compensator models are incorporated into both traditional and voltage stability constrained optimal power flow problems to study the effect that the different models have on costs and system load-ability. The proposed models are compared to typical models by means of a detailed analysis of the results obtained for two IEEE test systems; interior point methods are used to obtain numerical solutions of the associated optimization problems.**

Keywords— **Optimal Power Flow, Modeling, Voltage Stability, Interior Point Methods.**

I. Introduction

AS OPEN access market principles are applied to power systems, an increased emphasis on using accurate optimal power flow techniques will arise, as power systems will have to be operated at higher loading conditions, with market influences demanding greater attention to operating cost versus stability margins. Furthermore, it is shown in [1], [2], [3] that traditional models may fail to accurately represent power systems in certain conditions, especially near stability limits. Hence, this paper examines the effects of detailed generator models, exponential load models, and a "power flow" SVC model in traditional Optimal Power Flow (OPF) and Voltage Stability Constrained Optimal Power Flow (VSC-OPF) problems. The various VSC-OPF problems considered here are based on the optimization formulations proposed in [4], [5], [6].

A detailed generator model is incorporated into OPF problems to improve the accuracy of the results. It is shown in [2] that reactive power limits play a significant role in discrepancies between detailed and non-detailed generator models. Furthermore, in [7], [8], [9], [10], it is demonstrated that reactive power limits play a significant role in voltage collapse of power systems. Therefore, particular attention is placed here to the modeling of reactive power limits in generators to study their effects on various OPF solutions.

Load modeling represents a key mechanism in stability analysis [1]; therefore, various load models are considered in this paper. Specifically, voltage dependent load models are included into traditional OPF and VSC-OPF problems to study their effect on costs and stability margins.

Finally, because of its influence in voltage stability, a Static VAR Compensator (SVC) model is also incorporated into various OPF formulations. These controllers provide reactive power compensation, increasing the maximum transfer capability of a power network [11], [12]. Hence, the steady-state model for SVC controller proposed in [11] is included here into various OPF problems to determine the effect of this device on the optimal solutions.

This paper is structured as follows: In Section II, a review of voltage stability and the VSC-OPF problems are presented. In Section III, the generator, exponential load and SVC models used in this paper are briefly discussed. Numerical results obtained from the application of the interior point methodologies proposed in [13] to the traditional OPF and several VSC-OPF problems are presented and discussed in Section IV, based on simulations carried out on the IEEE 57-bus and 118-bus test systems. In Section V, a summary of the main conclusions and contributions of the paper is presented.

II. Background Review

The basic background behind the traditional OPF problem and the addition of voltage stability constraints to the problem is briefly discussed in this section.

Some fundamental concepts behind voltage stability analysis are briefly discussed first to better understand the application of optimization techniques to voltage collapse based problems.

A. Voltage Stability and Bifurcation Theory

Nonlinear phenomena, especially certain types of bifurcations, have been shown to be responsible for a variety of stability problems in power systems (e.g., [14]). In particular, the lack of post contingency equilibrium points, typically associated with Saddle-node bifurcations (SNBs) and certain types of Limit-induced Bifurcations (LIBs), have been shown to be the main reason behind several voltage collapse problems throughout the world. Detailed explanations and examples of these bifurcations in power systems and their association with voltage stability can be found in [10].

Accepted for publication in *IEEE Tans. Power Systems*, August 2002.

This research has being supported by the National Sciences and Engineering Research Council (NSERC) of Canada.

W. Rosehart is with the Dept. Electrical & Computer Eng., University of Calgary, Calgary, AB, Canada, T2N 1N4, rosehart@ieee.org

C. A. Cañizares and V. H. Quintana are with the Dept. Electrical & Computer Engineering, University of Waterloo, Waterloo, ON, Canada, N2L 3G1, C.Canizares@ece.uwaterloo.ca, quintana@kingcong.uwaterloo.ca

In general, bifurcation points can be defined as equilibrium points where changes in the "quantity" and/or "quality" of the equilibria associated with a nonlinear set of dynamic equations occur with respect to slow varying parameters in the system [15]. Since power systems are modeled by sets of nonlinear differential equations, various types of bifurcations are generically encountered in these systems as certain parameters vary.

Given the nonlinear nature of the system and its associated equations, the system typically has multiple equilibrium points. Of interest are the equilibrium points and parameter values where the system goes from being stable to unstable, from being unstable to stable, or where the number of equilibrium points changes with respect to the bifurcation parameters, which are here referred to as λ; these points are defined as bifurcation points. These bifurcations are mathematically characterized by the eigenvalues of the system Jacobian changing [16]. Thus, when two equilibrium points "merge" and one of the eigenvalues becomes zero, one has a saddle-node (SNB), a transcritical or a pitchfork bifurcation; when a conjugate pair crosses the imaginary axis, one has a Hopf bifurcation (HB). Generally, one can expect to encounter SNBs or HBs as the bifurcation parameters change, as transcritical and pitchfork bifurcations can only occur if the system contains some particular "symmetries" [14].

In power systems, control limits, in particular control limits associate with generator reactive power limits, have been shown to yield special bifurcations known as LIBs [17]; these bifurcations are also generic, i.e., are typically encountered in power systems. Certain types of LIBs are characterized by two merging equilibrium points and an instantaneous "jump" of the eigenvalues from the left-half plane to the right-half plane; there are no singularities associated with this bifurcation. As in the case of SNBs, in these LIBs, the system equilibria locally disappear for an additional increase or decrease, depending on the direction of change, of the bifurcation parameters λ. For example, when reactive power limits of certain generators are reached, no local equilibria may exist for increased loading conditions [10].

Voltage collapses have been shown to be strongly connected to SNBs and some LIBs [10]. As the system approaches the SNB/LIB point, also referred to as the voltage collapse point, the stability region of the system decreases until it becomes zero at the SNB/LIB point, resulting in a system collapse due to lack of equilibria [18]. Thus, a voltage stability margin is defined as the "distance", with respect to the bifurcation parameters λ, from the "current" operating point to the voltage collapse or SNB/LIB point; the system is assumed to be voltage secure if this margin is "reasonably" greater than zero. In practical systems, operators would be interested in maintaining the system with a given voltage stability margin, so that realistic contingencies do not make the system unstable [10].

When operational limits that are not directly linked to system controls, such as bus voltage or transmission line limits, are considered in voltage stability analysis, and these limits are the constraints that define the voltage stability margin of the system, the associated equilibrium point does not correspond to a collapse point, since the system still presents equilibrium points beyond these limits, i.e. equilibria do not locally disappear due to these types of limits. For this reason, in this paper the operating point at which a SNB, a LIB or an operational limits are reached will be referred to as a maximum loading point instead of a collapse point, since the bifurcation parameters λ are typically associated with the system loading conditions, as explained in more detail below.

B. OPF Formulations

In general, the traditional OPF problem can be readily modified to include voltage stability criteria by changing the objective function and adding some additional constraints as follows [4], [5], [6]:

$$\begin{aligned} \min \quad & G(x_p, \rho, \lambda_p, \lambda_*) \\ \text{s.t. :} \quad & F(x_p, \rho, \lambda_p) = 0 \\ & F(x_*, \rho_*, \lambda_*) = 0 \\ & \underline{H_p} \le H(x_p) \le \overline{H_p} \\ & \underline{H_*} \le H(x_*) \le \overline{H_*} \\ & \underline{x_p} \le x_p \le \overline{x_p} \\ & \underline{x_*} \le x_* \le \overline{x_*} \\ & \underline{\rho} \le \rho \le \overline{\rho} \\ & \underline{\rho_*} \le \rho_* \le \overline{\rho_*} \end{aligned} \tag{1}$$

where the subscripts p and $*$ indicate the current and maximum loading points, respectively. $G(x_p, \rho, \lambda_p, \lambda_*)$ is the objective function to be minimized, which has an OPF component, i.e., production costs or loses, that may be dependent on (x_p, ρ, λ_p), and a voltage stability component that is a function of λ_* and possibly of λ_p, as discussed below. $F : \Re^n \to \Re^m$ generally represents the power flow equations; and $H : \Re^n \to \Re^p$ usually represents transmission line limits, with lower and upper limits represented by $\underline{H}$ and $\overline{H}$, respectively. It is assumed that the inequality constraints defined by the limits on $H(x_p)$, $H(x_*)$, x_p, and x_* can be separated into separate constraints at the current and maximum loading points. For the basic OPF model considered in this paper, the vector of dependent system variables $x = \{V_l, \delta, Q_g\} \in \Re^n$, where l stands for the set of load buses and g represents the set of generator buses; their lower and upper limits are represented by $\underline{x}$ and $\overline{x}$, respectively. The power system independent or control variables $\rho = \{V_g, P_g, a\}$, where a represents the tap settings of the under-load tap changing transformers; the lower and upper limits on ρ are represented by $\underline{\rho}$ and $\overline{\rho}$, respectively. Finally, $\rho_* = \{V_{g*}, P_{g*}(P_g, K_{g*}), a_*\}$ maps the control variables at the current operating point, defined by p, into the maximum loading point to account for generation changes, since $K_{g*} \in \Re$ is a scalar used to model a distributed slack bus as follows:

$$P_{g*} = P_g(1 + K_{g*}) \tag{2}$$

The constraints in (1) define $*$ as a SNB, a LIB or an operational limits point, depending on which limits are active at the corresponding maximum loading point. The proof of this is based on the KKT optimality conditions of (1) and is discussed in detail in [6].

It is important to highlight the fact that in (1), λ stands for only one parameter instead of several, contrary to what is proposed in [19], i.e., the optimization is done in a particular direction of load change. This is not a problem, given that the optimization would be typically done several times a day during the operation of the system, as in the case of any other OPF procedure. This assumption simplifies the numerical solution process of the optimization problem, which is already a difficult numerical problem, given the highly nonlinear behavior of the system constraints and the effect of limits associated with the inclusion of the maximum loading conditions $*$.

Depending on the definition of the objective function $G(\cdot)$ in (1), one can pursue different optimization strategies and hence obtain solutions to a variety of distinct problems, as discussed in [4], [5], [6]. In this paper, only the particular VSC-OPF problems of Maximum Voltage Stability Margin (MVSM) and Fixed Voltage Stability Margin (FVSM) are considered and discussed.

B.1 Traditional OPF

For the traditional OPF, the objective function is defined as the following quadratic function:

$$G(P_g) = \sum_g a_g \; P_g^2 + b_g \; P_g + c_g \tag{3}$$

where a_g, b_g and c_g are constants that define the generator g costs.

B.2 Maximum Voltage Stability Margin (MVSM)

The MVSM problem with constraints incorporated on the current and critical loading point [6], [20], is a particular example of (1). The objective function in this case can be written as

$$G(\lambda_p, \lambda_*) = -(\lambda_* - \lambda_p) \tag{4}$$

where $\lambda_* > \lambda_p > 0$. The main idea here is to maximize the distance to a SNB, LIB or operational limits point, while guaranteeing the feasibility of the "current" operating point x_p associated with the load level defined by λ_p, as well as the feasibility of all control and operational limits. For example, increasing generator voltage magnitude settings generally increases the distance to a maximum loading point, improving voltage security, but under lighter loading conditions, higher voltage settings may lead to over-voltages. Incorporating the current operating point into the optimization problem can eliminate this problem; however, it also reduces the space of feasible solutions.

B.3 Fixed Voltage Stability Margin (FVSM)

An alternative approach to accounting for voltage stability in the OPF problem is to include a voltage stability inequality constraint. In this formulation, the objective function is the traditional OPF cost minimization defined in (3) with the following equality constraint added to (1):

$$\lambda_* - \lambda_p \geq \Delta\lambda_{min} \tag{5}$$

where $\Delta\lambda_{min}$ represents the minimum acceptable margin of stability for the system, which is defined by the system operator.

III. System Modeling

A. Detailed Generator Model

As loading levels in power systems increase, the effect of generator models increases. Simplified models seldom incorporate their nonlinear characteristics and parameter limits properly. The usual treatment of generators as PV buses may lead to unreliable results in certain types of system analyses. It should be pointed out, that since generator reactive power limits are directly incorporated into the OPF formulations, the term PV generator model also considers PQ generator models, since in the optimization problem, P_g, V_g and Q_g are all free to change, subject to the constraints placed on them. Since limits of the armature current and field voltage accurately reflect the true limits of generators, their inclusion in the standard power flow equations should enhance the model. Therefore, a detailed model of the generator is used in the traditional OPF and VSC-OPF problems discussed in the previous section.

The model of the synchronous generator used in this section is based on the detailed model presented in [21]. It is assumed that the field current is proportional to the magnitude of the induced voltage and saturation can be neglected. The following equations are used here to describe the dq-axis generator model in a synchronously rotating reference frame:

$$\begin{aligned} E_f - V_q &= R_a I_q - X_d I_d \\ -V_d &= R_a I_d + X_q I_q \\ V_g &= \sqrt{V_d^2 + V_q^2} \\ I_a &= \sqrt{I_d^2 + I_q^2} \\ P_g &= V_q I_q + V_d I_d \\ Q_g &= V_q I_d - V_d I_q \end{aligned} \tag{6}$$

where I_d and I_q are the direct and quadrature components of the armature current I_a; V_d and V_q are the direct and quadrature components of the terminal voltage V_g and; R_a and X_d and X_q are the armature resistance and direct and quadrature synchronous reactances, respectively. The real and imaginary power injected into the transmission system by the generator is given by P_g and Q_g respectively. For this model, x in (1) includes the variables E_f, V_d, V_q, I_d, I_q, and I_a, besides V_g and Q_g for each generator, with constraints in E_f and I_a as explained below.

The two main windings in the machine, i.e., the armature and field windings, must be protected from overheating. The heating of the armature winding is associated

with its current; therefore, the protection of the armature winding is implemented by limiting the magnitude of the armature current I_a. If the terminal voltage is considered constant, then the armature current effectively sets the apparent power rating of the generator, $\tilde{S}_g = \tilde{V}_t \tilde{I}_a^*$.

In the same manner, the maximum allowable heating of the field winding sets the maximum field current. Since the field voltage E_f is directly proportional to the field current, the field winding limit can be expressed as a limit on E_f.

Based on capability curves [12], [22], [23], the maximum and minimum armature current and field voltage are defined according to

$$\begin{bmatrix} I_{a\,max} \\ I_{a\,min} \\ E_{f\,max} \\ E_{f\,min} \end{bmatrix} = \begin{bmatrix} \frac{1}{V_{min}}\sqrt{Q_{max}^2 + P_{max}^2} \\ 0.0 \\ \frac{1}{V_{min}}\sqrt{(Q_{max} + \frac{V_{t\,max}^2}{X_d})^2 + P_{max}^2} \\ 0.0 \end{bmatrix} \quad (7)$$

Since there is no one-to-one mapping between the limits for the proposed model and the traditional PV model for all loading levels, this approximation is seen adequate to demonstrate the differences in the two models.

B. Load Models

Because of the use of aggregate methods to represent loads, standard PQ models may not accurately reflect the characteristic of the system in all cases. In this section, different static load models that express the active and reactive powers of loads as a function of the voltage magnitude at the load bus are considered.

Several voltage dependent load models have been analyzed in voltage stability studies, for example [1], [23]. In this paper, an exponential load model is introduced in the various OPF formulations. This model represents the power demand of the load as a function of its terminal voltage as follows:

$$\begin{aligned} P_l &= P_{lo}\left(\frac{V_l}{V_{lo}}\right)^{\varrho_1} \\ Q_l &= Q_{lo}\left(\frac{V_l}{V_{lo}}\right)^{\varrho_2} \end{aligned} \quad (8)$$

where P_{lo} and Q_{lo} are the reference real and reactive powers consumed at a reference voltage V_{lo}. The exponents ϱ_1 and ϱ_2 depend on the type of load that is being represented. Thus, for a constant impedance model $\varrho_1 = \varrho_2 = 2$; for a constant current model $\varrho_1 = \varrho_2 = 1$; and for a constant power model $\varrho_1 = \varrho_2 = 0$. In this case, P_l and Q_l are added to x in (1), with no limits in their values.

C. Static VAR Compensator (SVC)

Since the early eighties, advances in Flexible AC Transmission Systems (FACTS) controllers in power systems have led to their application in improving stability of power networks [24]. Several studies analyzing the application of FACTS controllers for voltage and angle stability have been reported in the literature (e.g., [11]). The effect of the SVC controller on the economic operation and voltage stability

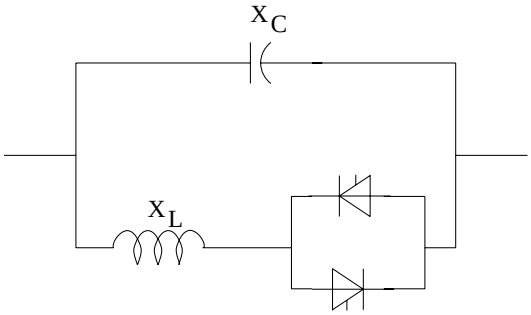

Fig. 1. Common structure for SVC.

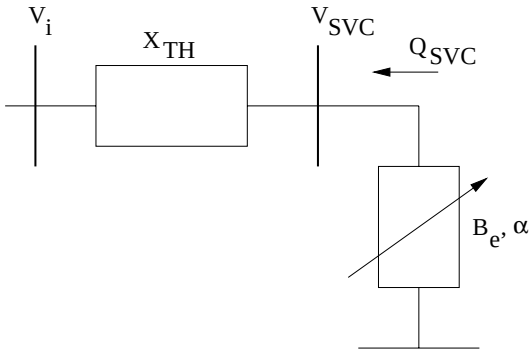

Fig. 2. SVC steady state circuit representation.

of the network is the principle motivation behind incorporating the SVC into various OPF formulations.

The steady state model proposed in [11] is used here to incorporate the SVC in the OPF problems of interest. This model is based on representing the controller as a variable impedance, assuming a SVC configuration with a Fixed Capacitor (FC) and Thyristor Controlled Reactor (TCR) as depicted in Fig. 1. In this case, if the SVC bus voltage is assumed sinusoidal, a Fourier analysis on the inductor current waveform can be used to demonstrate that the fixed reactor and bi-directional valve can be modeled as an equivalent variable reactance X_e of value:

$$X_e = \frac{\pi X_L}{\sin 2\alpha - 2\alpha + \pi(2 - \frac{X_L}{X_C})} \quad (9)$$

where X_L and X_C are the fundamental frequency reactance of the inductor and capacitors depicted in Fig. 1, and α is the firing angle of the valves with respect to the positive zero crossing of the controller voltage. The model incorporated in the different OPF implementations is written in terms of the equivalent susceptance, $B_e = -1/X_e$, rather than the corresponding reactance equations, based on numerical performance as discussed in [11].

The SVC is usually connected to the transmission system through a step-down transformer, which can be treated as other transformers in the system. A steady state circuit representation of the connection of the SVC through a step-down transformer is illustrated in Fig. 2, where V_i is the magnitude of the voltage at the bus which the SVC controls, V_{SVC} is the voltage across the controller, X_{TH} is the impedance of the step-down transformer, and

$Q_{SVC} = V_{SVC}^2 B_e$ is the reactive power that the SVC injects into the power network.

The typical steady state control characteristics of the SVC when $\alpha_{\min} \leq \alpha \leq \alpha_{\max}$ (when α exceeds this limits, the SVC loses voltage control) can be represented as

$$V_{SVC} = V_{REF} + X_{SL} I_{SVC} \tag{10}$$

where V_{REF} is a reference voltage for the controller, X_{SL} is the SVC control slope, and $I_{SVC} = V_{SVC} B_e$.

In terms of the different OPF formulations used in this paper, the SVC model introduces in (1) four new dependent variables and one additional independent variable. Thus, the current I_{SVC}, reactive power Q_{SVC}, firing angle α, and equivalent conductance B_e are added to x; the voltage reference V_{REF} is added to ρ. Constraints are only placed in α for this model.

IV. Numerical Analysis

The effect of incorporating the detailed generator model, static load models, and the SVC model into the traditional OPF and VSC-OPF problems is analyzed here by analyzing the results of solving these problems for the IEEE 57-bus and 118-bus test systems. To determine both the effect of the models and the effect of limits and loading conditions on the different OPF formulation solutions, the analysis is done at several loading levels, with and without limits on generation and bus voltage magnitudes.

For the analysis presented in this section, the OPF problem is modeled using the generic formulation presented in (1). The two VSC-OPF formulations discussed in Section II are compared to the traditional OPF (minimization of operating costs). All these formulations are nonlinear programming problems since the constraints are nonlinear. The objective function for the MVSM problem is linear, whereas for the traditional OPF and the FVSM formulation the objective function is quadratic, as discussed in Section II.II-A. The constraints incorporated into each of the cases include, bus voltage limits, transmission line limits, generator real and reactive power limits and transformer tap limits. These constraints are incorporated at both the current and the critical loading point when considering the VSC-OPF formulations. Additional constraints, as discussed in Section III, are incorporated when using the detailed generator, load and Static VAR Compensator models.

Load changes are modeled as follows in all OPF formulations:

$$\begin{aligned} P_{l_\lambda} &= \lambda\, P_l \\ Q_{l_\lambda} &= \lambda\, Q_l \end{aligned} \tag{11}$$

where λ is the bifurcation or loading parameter, and P_l and Q_l are either constant values or the variables defined in (8) for the load model studies.

Based on the algorithm presented in [25], a nonlinear primal-dual predictor-corrector interior point method written in MATLAB is used to perform the numerical analysis. Simulations are performed considering various operational limits at both the current operating point p and the maximum loading point $*$. The maximum loading points found in the numerical results tended to correspond to LIBs or operational limits rather than SNBs, which is to be expected since limits where placed on the maximum loading point $*$.

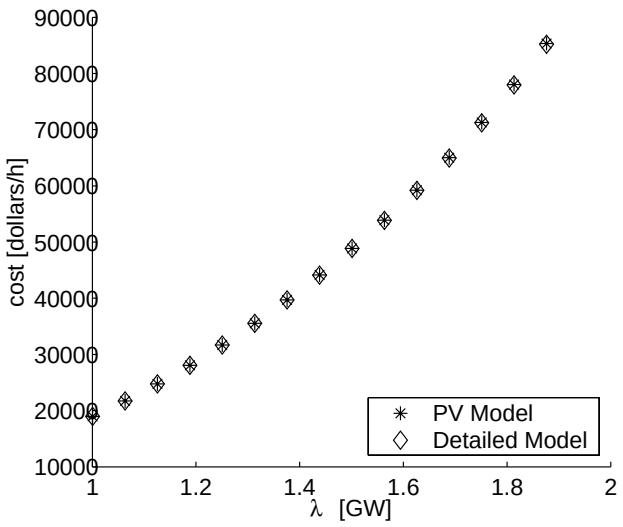

Fig. 3. Cost versus current loading point for the 57-bus system when minimizing cost in the traditional OPF for the PV and detailed generator models.

A. Detailed Generator Model

The difference between the detailed generator model and the traditional PV model is first compared for a traditional OPF problem. A plot of the cost versus loading level when using the two models for the 57-bus system is shown in Fig. 3. For all loading levels, the costs for the two models are rather similar. But at higher loading levels, as reactive power limits for the PV generator model become active, the detailed generator model yields lower costs, as shown in Fig. 4. The dashed line in Fig. 4 shows the percent reduction in operating cost when using the detailed generator model versus the traditional PV generator model when solving the FVSM problem. Similarly, the solid line in Fig. 4 shows the percent reduction in operating cost when using the detailed generator model versus the traditional PV generator model when solving the traditional OPF problem. In both cases, the traditional model provides a conservative estimate, and although the difference seems to be small in relative terms, it can easily add up to significant amounts in real terms. It is important to highlight the fact that the difference is several orders of magnitude higher than the tolerance of the optimization convergence criteria used.

A plot of the maximum loading level (λ_*) versus the current operating point (λ_p) when solving the MVSM formulation is shown in Fig. 5. In general, for all loading levels, the PV and detailed generator model have similar characteristics, but using the detailed generator model resulted in general in a higher maximum loading level. For

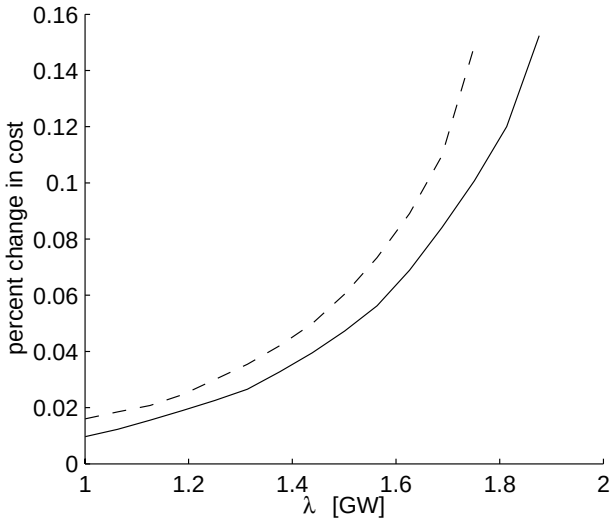

Fig. 4. Reduction in total operating cost for the 57-bus system between the detailed and PV generator models for the FVSM (dashed line) and traditional OPF formulations (solid line).

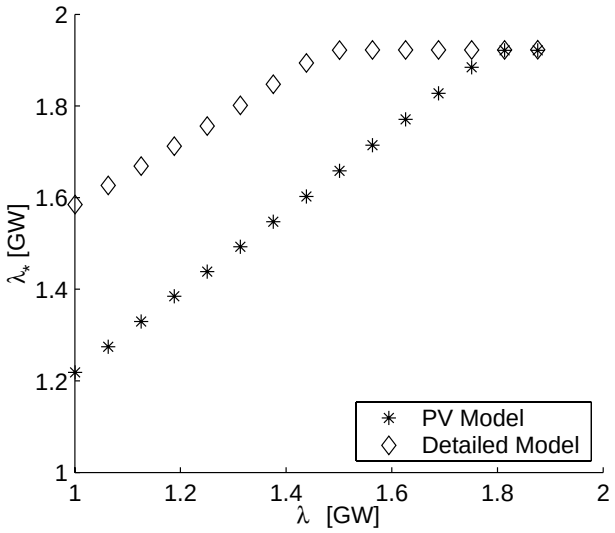

Fig. 5. Maximum loading versus current loading point for the 57-bus system when solving the MVSM formulation for the PV and detailed generator models.

both models, at lower loading levels, upper voltage limits for some non-generator buses at the current operating point limited raising generator voltage settings, which in turn reduced the maximum loading level. As the current loading level is increased, these bus voltages decrease, allowing the generator voltage settings to increase, which in turn results in a higher maximum loading level. For the PV generator models, reactive power limits limit the maximum loading level; for detailed generation models, on the other hand, current limits define the maximum loading levels, thus yielding higher values in general. For both models, limits on active power eventually define a fixed upper limit on the maximum loading level λ_*, which explains why the maximum loading level of the two models converge at higher values of λ_p.

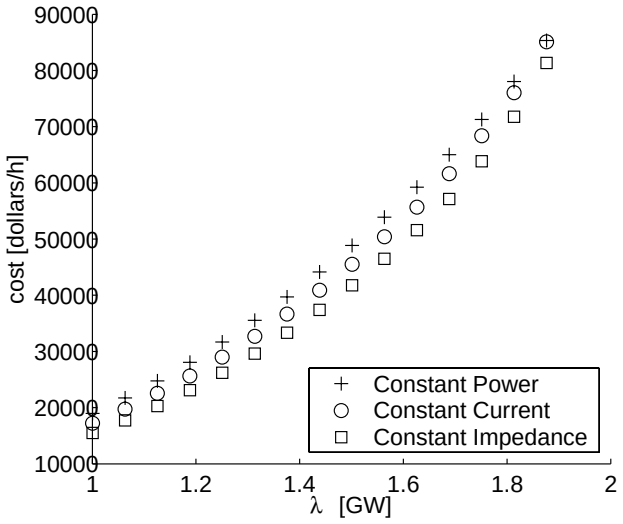

Fig. 6. Cost versus current loading point for the 57-bus system when solving the traditional OPF problem for different load models.

Similar results were obtained for the 118-bus test system.

B. Exponential Load Models

In traditional voltage stability analysis, constant impedance and current load models tend to have larger stability margins than constant power. This is attributed to the fact that the actual power consumption of the load decreases as the bus voltage decreases for both constant current and impedance models, resulting in a less stressed system.

The different load models are first incorporated into the traditional OPF problem (i.e., the OPF problem with no stability constraints). A plot of the cost versus loading level using the three load models for the 57-bus system is shown in Fig. 6. For all loading levels, the constant impedance model results in the lowest cost, followed by the constant current model, and finally the constant power model. Generator voltage settings for the constant current/impedance models tend to be low to reduce the amount of power absorbed by the loads. With the constant power load model, the generator voltage levels tend to be higher to reduce loses in the lines. The relative cost differences for the three models do not change greatly with increased loading.

Next, the MVSM formulation is applied to both test systems. Figure 7 shows the plot of the maximum loading level λ_* versus the current operating point λ_p for the 57-bus when solving the MVSM formulation with full operational limits at the maximum loading point. For all three load models, the maximum loading level λ_* increases as the current operating point λ_p is increased, a characteristic previously noticed and explained. The observed behavior of the voltage dependent loads (constant current and impedance loads) is due to the interaction between limits becoming active and the voltage dependency of the loads. When using these load models, the solution to the problem tends to lower voltage levels to reduce the power levels of the loads. However, bus voltages reaching lower limits at

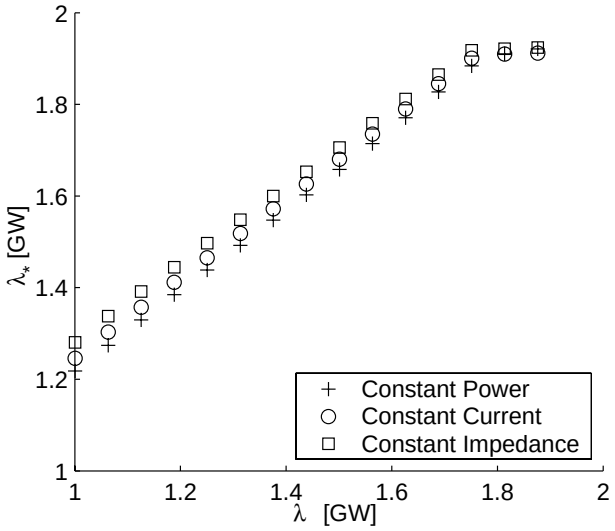

Fig. 7. Maximum loading versus current loading point for the 57-bus system when solving the MVSM formulation for different load models.

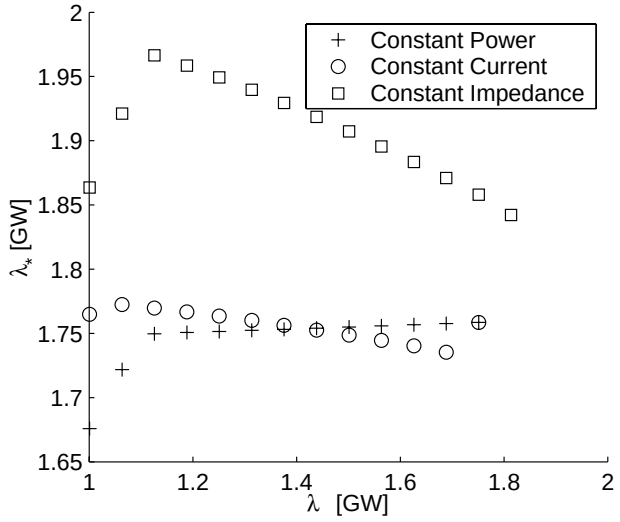

Fig. 8. Maximum loading versus current loading point for the modified 57-bus system when solving the MVSM formulation with generator real and reactive power limits at the critical point for different load models.

the maximum loading point λ_* force increases in voltage settings at the current operating point, resulting in some non-generator buses at the current operating point reaching upper voltage limits, similar to the behavior observed when using constant power load models.

The effect of limits on the behavior of the MVSM formulation is further illustrated by modifying the voltage limits of the 57-bus system to the limits proposed in [26]. Generally, the modified 57-bus system has higher maximum voltage limits and lower minimum voltage limits than in the original data; some of the reactive power limits are higher, but the reactive power limit for one of the generators is substantially reduced. No changes were applied to the active power limits.

Figure 8 illustrates the results obtained by applying the MVSM formulation to the modified 57-bus system with only generator real and reactive power limits at the maximum loading point. For lower loading levels, all three load models exhibit similar behavior as the original system. However, as the current loading point is increased, the MVSM starts to decrease for the constant current and constant impedance models. This behavior can be explained as follows: When using constant current and impedance models, lower limits on the voltage at the current loading level tend to limit the MVSM. As the loading level increases, generator voltage levels have to be increased to prevent voltage levels at non-generator buses from becoming too low at the current point. But increased generator voltage levels result in increased reactive power output from the generators (especially at the maximum loading point); the increased reactive power demand results in a lower stability margin as reactive power limits are reached (generator at Bus 1). For the constant current and constant impedance models, all the solutions obtained without voltage limits on the maximum loading point had one load bus voltage at a minimum setting. For any increases in load, this bus voltage would drop below an acceptable operating level. When using the constant power load model, power limits at the maximum operating point are reached at about $\lambda_p = 1.75$ GW, thus limiting any further increases in the maximum loading point.

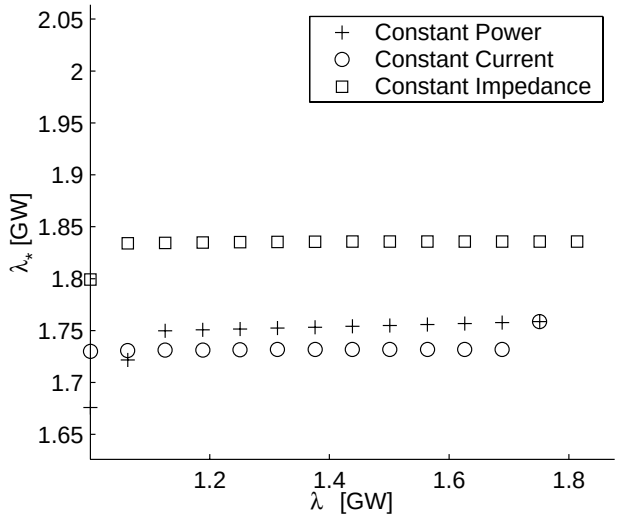

Fig. 9. Maximum loading versus current loading point for the modified 57-bus system when solving the MVSM formulation with operational limits at the critical point for different load models.

The effect of incorporating operational limits on the maximum loading point λ_* is shown in Fig. 9 when solving the MVSM formulation for the modified 57-bus system. For all three load models, incorporating lower voltage limits at the maximum loading point results in lower values of λ_*, but ensures that all loading points between the current and the maximum operating level are acceptable operating points. When using constant impedance load models, at low loading levels, similar characteristics as before are observed; a limit on a generator's reactive power output at

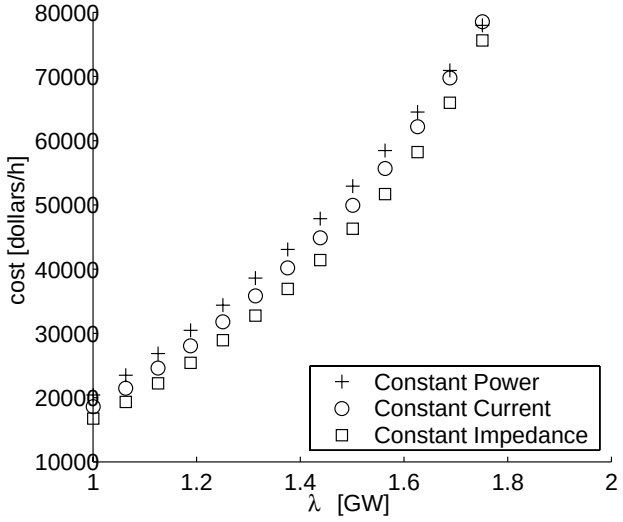

Fig. 10. Total operating cost for the different load models when solving the FVSM formulation for the 57-bus system.

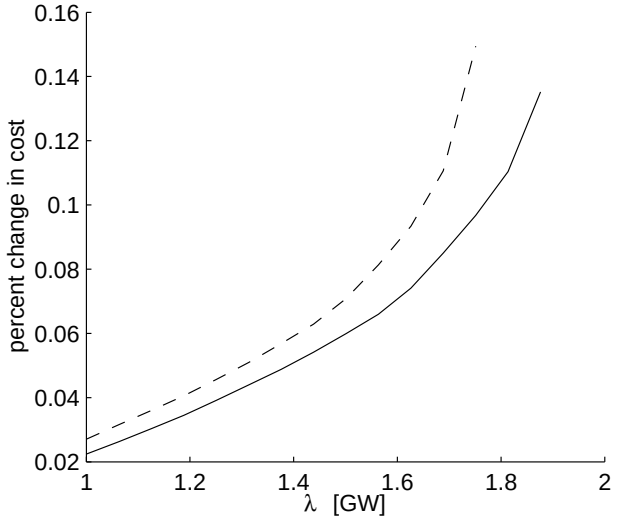

Fig. 11. Difference in total operating costs for the 57-bus system with a SVC versus no SVC when solving the traditional OPF (solid line) and the FVSM formulation (dashed line) with operational limits at the maximum loading point.

the maximum loading point is reached at about $\lambda_p = 1.85$ GW, and no further improvements can be made to optimize the maximum loading point, with the MVSM remaining constant for larger values of λ_p. For the constant current model, all generator reactive power upper limits are reached with the generator settings at the initial loading point, causing the value of λ_* to remain constant for all remaining values of λ_p. The negative slope of λ_* versus λ_p does not appear, because no voltages at the current loading point are at lower limits, as that would imply that those bus voltages would be below their operational limits at the critical loading point.

Figure 10 is a plot of the total operating costs when solving the FVSM formulation for the three load models. As expected, the characteristics are similar to those obtained when using the traditional OPF problem, the only difference is that, for a given loading condition λ_p, the costs are higher, as expected, since the system is now forced to maintain a minimum distance to a maximum loading point.

Similar results were obtained for the 118-bus test system.

C. Static VAR Compensator

Finally, the power flow SVC model is incorporated into both the traditional OPF and the VSC-OPF formulations. A SVC model was placed at one of the buses (Bus 31) of the 57-bus system using the SVC data presented in [11]. The SVC placement is chosen based on the eigenvectors of the zero eigenvalue at a SNB or the "tangent" vector at a LIB at the maximum loading point, as explained in detail in [11].

Figure 11 shows the difference in total operating costs for the 57-bus system with the SVC controller in the system versus no SVC when solving the traditional OPF problem. As expected, the effect of the SVC on reducing operating costs is more significant at higher loading levels.

The effect of the SVC controller on the maximum loading level of the system when solving the MVSM formulation, with no limits being enforced at the maximum loading point, is illustrated in Fig. 12. As depicted, the SVC significantly increases the loadability of the system. Figure 13 shows the results obtained when enforcing limits at the maximum loading point for the MVSM formulation. For all loading points the SVC enhances the stability margin, but the amount of improvement decreases because of limits. This further illustrates the significant effect of limits on these types of problems.

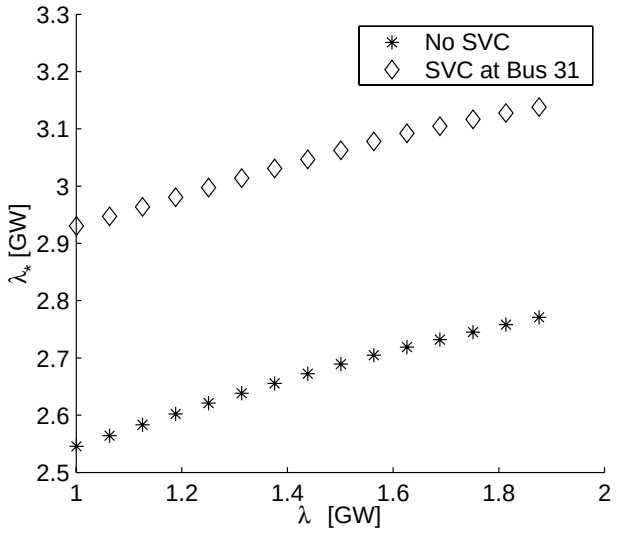

Fig. 12. Difference in maximum loading point for the 57-bus system with a SVC versus no SVC when solving the MVSM formulation with no limits at the maximum loading point.

Incorporating the SVC controller into the FVSM formulation resulted also in reduced costs, as shown in Fig. 11. However, observed that the benefits of incorporating the SVC are greater in this case than in the traditional OPF problem.

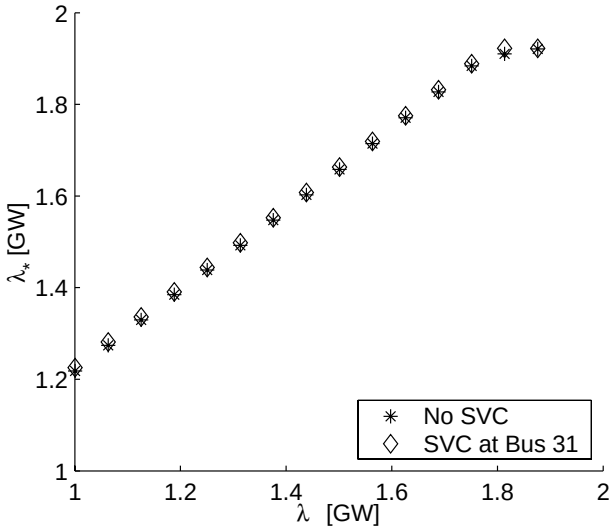

Fig. 13. Difference in maximum loading point for the 57-bus system with a SVC versus no SVC when solving the MVSM formulation with operational limits at the maximum loading point.

Similar results were obtained for the 118-bus system.

V. Conclusions

In this paper, a detailed generator model is incorporated into the traditional OPF and VSC-OPF problems. The effect of the different generator models on the total operating costs and stability margins for a couple of test systems is studied, resulting in the detailed generator model yielding lower costs and higher margins.

Three static load models are also analyzed when applied to the traditional OPF and VSC-OPF problems. The characteristics of the load models and their effect on costs and stability margins for different operational limits are analyzed through the results obtained for various case studies. In the VSC-OPF problems, it is observed that the lowering of generator voltage settings to reduce generator power output when using constant impedance and constant current load models leads to the need for including full operational limits on the current and the maximum loading point.

Finally, a power flow SVC model is incorporated into both the traditional OPF and the VSC-OPF formulations. It is shown that adding a SVC to the system results in lower operating costs, especially at higher loading levels. Furthermore, and as expected, the SVC improved the system loadability and hence the stability margins; however, limits at the maximum loading point tend to reduce these stability "gains".

References

[1] C. A. Cañizares, "On bifurcations, voltage collapse and load modeling," *IEEE Trans. Power Systems*, vol. 10, no. 1, pp. 512–522, Feb. 1995.

[2] P. A. Löf, G. Andersson, and D. J. Hill, "Voltage dependent reactive power limits for voltage stability studies," *IEEE Trans. Power Systems*, vol. 10, no. 1, pp. 220–228, Feb. 1995.

[3] D. H. Popovic, I. A. Hiskens, Y. V. Makarov, and D. J. Hill, "Investigation of load-tap changer interaction," *Electrical Power and Energy Systems*, vol. 18, no. 2, pp. 81–97, 1996.

[4] W. Rosehart, *Optimization of Power Systems with Voltage Security Constraints*, Ph.D. thesis, University of Waterloo, Waterloo, Ontario, 2000.

[5] W. Rosehart, C. Cañizares, and V. H. Quintana, "Cost of voltage stability in electricity markets," Proc. of the 2000 IEEE/PES Summer Meeting, Seattle, Washington, July 2000.

[6] W. Rosehart, C. Cañizares, and V. H. Quintana, "Optimal power flow incorporating voltage collapse constraints," Proc. of the 1999 IEEE/PES Summer Meeting, Edmonton, Alberta, July 1999, pp. 820-825.

[7] I. Dobson and L. Lu, "Voltage collapse precipitated by the immediate change in stability when generator reactive power limits are encountered," *IEEE Transactions on Circuits and Systems–I: Fundamental Theory and Applications*, vol. 39, no. 9, pp. 762–766, Sept. 1992.

[8] A. A. P. Lerm, C. A. Cañizares, F. A. B. Lemos, and A. S. e Silva, "Multi-parameter bifurcation analysis of power systems," *Proceedings of the North American Power Symposium*, pp. 76–82, Oct. 1998, Cleveland, Ohio.

[9] C. A. Cañizares and F. L. Alvarado, "Point of collapse and continuation methods for large ac/dc systems," *IEEE Trans. Power Systems*, vol. 8, no. 1, pp. 1–8, Feb. 1993.

[10] C. A. Cañizares, editor, "Voltage stability assessment, procedures and guides," Tech. Rep., IEEE/PES Power System Stability Subcommittee, Available at http://www. power. uwaterloo. ca.

[11] C. A. Cañizares and Z. T. Faur, "Analysis of SVC and TCSC controllers in voltage collapse," *IEEE Trans. Power Systems*, vol. 14, no. 1, pp. 158–165, Feb. 1999.

[12] P. Kundur, *Power System Stability and Control*, McGraw Hill Publishing Company, New York, 1994.

[13] G. L. Torres and V. H. Quintana, "An interior-point method for nonlinear optimal power flow using voltage rectangular coordinates," *IEEE Transactions on Power Systems*, pp. 1211–1218, Nov. 1998.

[14] C. A. Cañizares and S. Hranilovic, "Transcritical and Hopf bifurcations in ac/dc systems," *Proc. Bulk Power System Voltage Phenomena III—Voltage Stability and Security*, pp. 105–114, Aug. 1994.

[15] R. Seydel, *From Equilibrium to Chaos—Practical Bifurcation and Stability Analysis*, Elsevier Science, North-Holland, 1988.

[16] C. A. Cañizares, "Conditions for saddle-node bifurcations in ac/dc power systems," *Int. J. of Electric Power & Energy Systems*, vol. 17, no. 1, pp. 61–68, Feb. 1995.

[17] V. Venkatasubramanian, H. Schättler, and J. Zaborsky, "Dynamics of large constrained nonlinear systems–A taxonomy theory," *Proceedings of the IEEE*, vol. 83, no. 11, pp. 1530–1561, Nov. 1995.

[18] C. A. Cañizares, "Calculating optimal system parameters to maximize the distance to saddle node bifurcations," *IEEE-Transactions on Circuits and Systems-I: Fundamental Theory and Applications*, vol. 45, no. 3, pp. 225–237, Mar. 1998.

[19] F. Alvarado, I. Dobson, and Y. Hu, "Computation of closest bifurcations in power systems," *IEEE Trans. Power Systems*, vol. 9, no. 2, pp. 918–928, May 1994.

[20] W. Rosehart, "Power system optimization with voltage stability constraints," Student poster session, 1998 IEEE/PES Summer Meeting, San Diego, CA, *IEEE Power Engineering Review*, Oct. 1998, pp. 14.

[21] J. Arrillaga, C. P. Arnold, and B. J. Harker, *Computer Modeling of Electric Power Systems*, John Wiley and Sons, Chichester, 1983.

[22] S. Chapman, *Electric Machinery Fundamentals, Third Addition*, McGraw Hill, New York, 1998.

[23] T. Van Cutsem and C. Vournas, *Voltage Stability of Electric Power Systems*, Kluwer Academic Publishers, Boston, 1998.

[24] N. G. Hingorani, "Flexible AC Transmission Systems," *IEEE Spectrum*, pp. 40–45, Apr. 1993.

[25] G. L. Torres and V. H. Quintana , "Nonlinear optimal power flow in rectangular form via a primal-dual logarithmic barrier interior point method," Tech. Rep. 96-08, University of Waterloo, 1996.

[26] G. L. Torres, *Nonlinear Optimal Power Flow by Interior and Non-Interior Point Methods*, Ph.D. thesis, University of Waterloo, Waterloo, Ontario, 1998.

William D. Rosehart received his Bachelors, Masters and Ph.D. degrees in Electrical Engineering from the University of Waterloo in

1996, 1997, and 2001, respectively. He is currently an Assistant Professor in the Department of Electrical and Computer Engineering at the University of Calgary. His main research interests are in the areas of numerical optimization techniques, stabilities issues and modeling power systems in a deregulated environment.

Claudio A. Cañizares received the Electrical Engineer Diploma from the Escuela Politécnica Nacional (EPN), Quito-Ecuador in 1984, where he was a Professor for several years. His MS (1988) and PhD (1991) degrees in Electrical Engineering are from the University of Wisconsin–Madison. Dr. Cañizares is currently an Associate Professor and the Associate Chair of Graduate Studies at the Department of Electrical & Computer Engineering of the University of Waterloo, and his research activities concentrate on modeling, simulation, and stability issues for ac/dc/FACTS power systems in a deregulated environment.

Victor H. Quintana received the Dipl. Ing. degree from the State Technical University of Chile in 1959, and the M.Sc. and Ph.D. degrees in Electrical Engineering from the University of Wisconsin, Madison in 1965, and University of Toronto, Ontario, in 1970, respectively. Since 1973 he has been with the University of Waterloo, Department of Electrical and Computer Engineering, where he is a full professor. His main research interests are in the areas of numerical optimization techniques, state estimation and control theory as applied to power systems.